Journal of Biomolecular NMR, 5 (1995) 25–36
ESCOM

J-Bio NMR 217

(H)NCAHA and (H)CANNH experiments for the determination of vicinal coupling constants related to the ϕ-torsion angle

Frank Löhr and Heinz Rüterjans*

Institut für Biophysikalische Chemie der Johann Wolfgang Goethe Universität Frankfurt am Main, Biozentrum, Marie Curie Strasse 9, D-60439 Frankfurt am Main, Germany

Received 4 May 1994
Accepted 8 July 1994

Keywords: 3D triple-resonance NMR; $^1H,^1H$ and $^1H,^{13}C$ J-coupling constants; E.COSY; ϕ-angle constraints; *Desulfovibrio vulgaris* flavodoxin

Summary

A set of three-dimensional triple-resonance experiments is described which provide $^3J_{H^NH^\alpha}$, $^3J_{H^NCO}$, $^3J_{H^NC^\beta}$ and $^3J_{H^\alpha CO}$ coupling constants. The pulse sequences generate E.COSY-like multiplet patterns and comprise a magnetization transfer from the amide proton to the α-proton or vice versa via the directly bound heteronuclei. For residues with the $^1H^\alpha$ spin resonating close to the H_2O signal, a modified HNCA experiment can be employed to measure the vicinal $^1H^N,^1H^\alpha$ couplings. Ambiguities associated with the conversion of $^3J_{H^NH^\alpha}$ values into ϕ-angle constraints for protein structure determination can be resolved with the knowledge of the heteronuclear ^3J-couplings. In favourable cases, stereospecific assignments of glycine α-protons can be obtained by employing the experiments described here in combination with NOE data. The methods are applied to flavodoxin from *Desulfovibrio vulgaris*.

Introduction

Estimates of torsion-angle contraints from vicinal scalar coupling constants are supplementary to NOE data for the determination of protein structures. In biomacromolecules the linewidths often exceed the coupling constants to be measured – a problem which in principle can be overcome by generating E.COSY-type (Griesinger et al., 1985,1986,1987) multiplet patterns. During the past few years a variety of NMR techniques (Montelione et al., 1989; Sørensen, 1990; Schmieder et al., 1991; Eggenberger et al., 1992a; Schwalbe et al., 1993; Weisemann et al., 1994a,b) have been developed for isotopically labeled proteins, exploiting large one-bond couplings to separate unresolved multiplet components along another frequency domain.

Constraints for the backbone angle ϕ may be derived from $^3J_{H^NH^\alpha}$ coupling constants which are available either from NMR methods based on the E.COSY principle (Schmieder et al., 1991; Seip et al., 1992; Görlach et al., 1993; Madsen et al., 1993; Weisemann et al., 1994a) or from cross peaks in HMQC (Kay et al., 1989) and NOESY and COSY (Ludvigsen et al., 1991) spectra. In a different approach, a quantitative evaluation of peak intensities in $^1H^N,^{15}N$ (Billeter et al., 1992) and $^1H^N,^1H^\alpha$ (Vuister and Bax, 1993) correlation spectra, where the $^3J_{H^NH^\alpha}$ coupling acts as a passive and an active coupling, respectively, leads to the determination of its size. However, since up to four dihedral angles correspond to one J-value (Karplus, 1959,1963), the conversion of a single coupling constant into structural information is not unambiguous.

As depicted in Fig. 1, apart from $^3J_{H^NH^\alpha}$, the ϕ-angle is also defined by three $^1H,^{13}C$ couplings for which Karplus parameters exist (Bystrov, 1976). The combined use of the four vicinal couplings has recently been demonstrated for a cyclic hexapeptide (Schmieder and Kessler, 1992). In this paper we will demonstrate that $^3J_{H^NH^\alpha}$, $^3J_{H^NCO}$, $^3J_{H^NC^\beta}$ and $^3J_{H^\alpha CO}$ coupling constants can be measured for a protein with a set of modified 3D (H)NCAHA and (H)CANNH (Montelione and Wagner, 1990; Kay et al., 1991; Boucher et al., 1992) experiments. The pulse sequences induce a magnetization transfer from ^{15}N to $^{13}C^\alpha$ or vice versa and correlate the chemical shifts of

*To whom correspondence should be addressed.

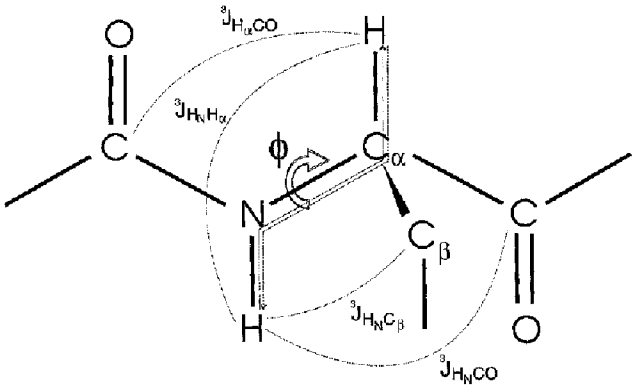

Fig. 1. Schematic representation of a peptide backbone fragment. The magnetization transfer pathways for intraresidual correlations provided by (H)NCAHA- and (H)CANNH-type experiments are given by broken arrows. Dotted lines indicate vicinal $^1H,^1H$- and $^1H,^{13}C$-couplings which supply information about the ϕ-torsion angle.

these nuclei with either the $^1H^\alpha$ or the $^1H^N$ resonance. One of the spins not involved in the magnetization transfer between the amide nitrogen and the α-carbon but directly bound to the nucleus which evolves as a function of t_1 is not decoupled during this period. As a consequence, the vicinal coupling between the passive spin and the proton detected in t_3 can be extracted from the displacement of the two submultiplets along F3.

Materials and Methods

The NMR experiments shown in Fig. 2 were carried out with a 2.2 mM sample of uniformly $^{13}C/^{15}N$-labeled, oxidized *Desulfovibrio vulgaris* flavodoxin in 0.5 ml 10 mM potassium phosphate buffer, pH = 7, containing 5% D_2O. Recombinant flavodoxin was isotopically labeled using a $^{13}C/^{15}N$-enriched protein hydrolysate mixture (Martek Corporation) and purified following a procedure described by Curley et al. (1991). All spectra were recorded at 27 °C on a Bruker AMX-600 spectrometer, equipped with a multichannel interface and a triple resonance probe tuned for ^1H, ^{13}C and ^{15}N. Experiments C and D were carried out with an external power amplifier (M3205, American Microwave Technology, Inc.) for the ^{13}C channel.

The following experiments were performed using the pulse sequences depicted in Fig. 2 (characteristic multiplet patterns are shown in Fig. 3).

(A) H^N-coupled (H)NCAHA

This experiment correlates ^{15}N backbone resonances with the $^{13}C^\alpha$ and $^1H^\alpha$ resonances of the same and the preceding amino acid residue, according to the magnetization transfer pathway described by Montelione and Wagner (1990). Chemical shift evolution of the ^{15}N and the $^{13}C^\alpha$ spins is allowed simultaneously with the build-up and refocusing of antiphase magnetization due to $^1J_{NC\alpha}$ and $^2J_{NC\alpha}$. The proton 180° pulse in the ^{15}N constant-time evolution period T_N is applied after a fixed delay $1/(4\ ^1J_{NHN})$, instead of being shifted parallel to the nitrogen 180° pulse. Therefore, a cosine modulation due to the $^1J_{NHN}$ coupling is observed in the ^{15}N dimension. The reverse $^{13}C,^1H$ INEPT transfer without perturbing amide proton spin states is achieved by inserting a 90°_x proton pulse prior to detection of $^1H^\alpha$, as proposed by Sørensen (1990). This allows measurement of vicinal $^1H^N,^1H^\alpha$ coupling constants from the F3 displacement of the two multiplet components separated by $^1J_{NHN}$ in the F1 dimension.

The 3D spectrum resulted from a 84 (real) × 38 (complex) × 1024 (real) data matrix recorded in 63 h with 32 scans per increment and acquisition times of 21.5, 12.6 and 111.6 ms in t_1, t_2 and t_3, respectively. Spectral widths were 1923 Hz in the F1 (^{15}N) dimension, 3012 Hz in the F2 ($^{13}C^\alpha$) dimension and 4587 Hz in the F3 ($^1H^\alpha$) dimension. Linear prediction and zero-filling were applied to yield 256 × 128 × 1024 real points after Fourier transformation.

(B) H^α-coupled HNCA

The measurement of $^3J_{HNH\alpha}$ couplings in a HNCA-type experiment has been reported previously (Schmieder et al., 1991; Wagner et al., 1991; Seip et al., 1992; Madsen et al., 1993; Weisemann et al., 1994a,b). In order to minimize multiplet distortions caused by relaxation effects during the $^1J_{NC\alpha}$ refocusing delay, nitrogen antiphase magnetization with respect to the amide proton is converted to proton nitrogen multiple-quantum coherence immediately following the $^{13}C^\alpha$ evolution period (Görlach et al., 1993). The 1-1 echo sequence (Sklenář and Bax, 1987) is used for selective excitation of amide protons.

The spectrum was recorded with 32 scans per increment and spectral widths of 1488 Hz in F1, 3164 Hz in F2 and 9091 Hz in F3. Acquisition times were 20.8 ms (32 complex data points), 14.8 ms (48 complex data points) and 112.6 ms (2048 real data points) in t_1, t_2 and t_3. After discarding the upfield half of the spectrum in the F3 dimension, the size of the absorptive part of the resulting 3D spectrum was 64 (F1) × 256 (F2) × 1024 (F3) points.

(C) CO-coupled (H)CANNH

The carbonyl-coupled (H)CANNH experiment relies on the same spin topology for the measurement of $^3J_{HNCO}$ as the recently published Soft-HNCA-COSY sequence (Weisemann et al., 1994a). The carbonyl spins are passively coupled during a constant-time $^{13}C^\alpha$ chemical shift evolution period, leading to a 55 Hz splitting in F1 due to $^1J_{C\alpha CO}$. Magnetization is relayed to the amide protons for detection via the amide nitrogens, thus permitting the heteronuclear vicinal coupling to be determined from F3 traces. To avoid perturbation of ^{13}CO spins, all pulses on aliphatic carbons, with the exception of the first 180°

pulse, are implemented as Gaussian cascades G3 and G4 (Emsley and Bodenhausen, 1990). Setting the duration of the constant-time evolution period T_C to $1/^1J_{C\alpha C\beta}$ removes the effect of this coupling from the F1 dimension. Since in an (H)CANNH-type experiment $^{13}C^{\alpha}$ transverse magnetization is generated in a single INEPT polarization transfer step from the directly attached protons, pulse sequence C is shorter and contains less pulses than the Soft-HNCA-COSY experiment, which starts with excitation of amide protons.

Spectral widths were 4310, 1852 and 4630 Hz in F1, F2 and F3, respectively. The spectrum was recorded as a 228 (t_1) × 60 (t_2) × 1024 (t_3) real data set with acquisition times of 26.5, 16 and 110.6 ms. Sizes of the real part of the 3D spectrum were 512 in the F1 domain, 64 in the F2 domain and 1024 in the F3 domain. The total measuring time, using 16 scans per increment, was 71.5 h.

(D) CO,H^{α}-coupled (H)CANNH

Both the $^3J_{HNCO}$ and the $^3J_{HNH\alpha}$ couplings can be measured in a combined (H)CANNH-type experiment, when proton decoupling is avoided and the $^1H^{\alpha}$ magnetization is returned to the z-axis prior to detection of the amide protons. The pulse sequence is virtually identical to a 3D version of a 4D experiment proposed by Sørensen (1990) for the determination of $^3J_{HNH\alpha}$. However, since in our sequence ^{13}C hard pulses are replaced by band-selective pulses on aliphatic carbons, the carbonyl carbons represent passive spins. As a consequence, the cross-peak patterns consist of four components with an in-phase splitting due to $^1J_{C\alpha CO}$ and an antiphase splitting due to $^1J_{C\alpha H\alpha}$ in F1.

Acquisition times in all dimensions as well as spectral widths in F2 and F3 were identical to those of the spectrum recorded with pulse sequence C. In F1, 208 (real) increments were acquired with a spectral width of 3906 Hz. The size of the absorptive part of the final 3D spectrum was 512 (F1) × 64 (F2) × 1024 (F3) points. For each increment 16 scans were accumulated, resulting in a measuring time of 64 h.

(E) C^{β}-coupled (H)CANNH

$^3J_{HNC\beta}$ couplings are accessible with an experimental scheme similar to pulse sequence C, provided that the chemical shift difference between the $^{13}C^{\alpha}$ and $^{13}C^{\beta}$ resonances of the same residue is sufficiently large to permit selective excitation of $^{13}C^{\alpha}$ resonances. Here, the $^1J_{C\alpha CO}$ coupling is refocused, whereas the $^1J_{C\alpha C\beta}$ coupling is allowed to evolve during t_1. To resolve this one-bond coupling of approximately 35 Hz, the $^{13}C^{\alpha}$ evolution period is implemented in a semi-constant-time manner (Grzesiek and Bax, 1993; Logan et al., 1993). The 180° pulses on carbonyl carbons, nitrogens and α-carbons are shifted with different rates during t_1, thereby removing the effect of the $^{13}C^{\alpha}$-^{13}CO scalar interaction and maintaining a fixed value for the duration of the $^{13}C^{\alpha}$,^{15}N magnetization transfer T_C. On the other hand, the $^{13}C^{\alpha}$ precession period is increased by a factor of $2(\chi^1-\chi^2)$, which is set to 1.76 in the present case. Thus, evolution of $^{13}C^{\alpha}$ chemical shifts and $^1J_{C\alpha C\beta}$ couplings can take place during a t_1 period of $1.76 \times T_C$. The pulse lengths of the G3 and G4 cascades on $^{13}C^{\alpha}$ are adjusted for a 600 MHz spectrometer to produce a uniform excitation over a bandwidth of ±1400 Hz while no perturbation of spins at offset frequencies larger than 2700 Hz can be observed. Therefore, vicinal $^1H^N$,$^{13}C^{\beta}$ coupling constants can be measured for amino acid residues with $^{13}C^{\beta}$ spins resonating upfield from approximately 42 ppm.

The 3D spectrum resulted from a 160 (complex) × 25 (complex) × 1024 (real) data matrix recorded in 85 h with 16 scans per increment. Acquisition times were 53, 16.5 and 110.6 ms in t_1, t_2 and t_3, respectively. The spectral widths covered 3012, 1453 and 4630 Hz in F1, F2 and F3. After linear prediction in F2 and zero-filling in all dimensions the size of the absorptive part of the spectrum was 512 × 64 × 1024 points.

(F) CO-coupled (H)NCAHA

The $^3J_{H\alpha CO}$ vicinal couplings can be measured from F3 ($^1H^{\alpha}$) traces when the relatively small one-bond ^{15}N,^{13}CO coupling constant is resolved in the ^{15}N domain of a (H)NCAHA experiment. Again, a semi-constant-time evolution period is employed to overcome resolution limitations imposed by an optimal duration of T_N for the ^{15}N,$^{13}C^{\alpha}$ magnetization transfer. The ^{15}N evolution is extended by a factor of $1/(1-\chi)$ over T_N. In the present application, T_N is set to 31 ms and $1/(1-\chi)$ is chosen to be 2.78. All pulses on aliphatic carbons have the shapes of Gaussian cascades G3 and G4. The decoupling of $^{13}C^{\alpha}$ nuclei during acquisition is achieved with an MLEV-16 expansion of G3 pulses (Eggenberger et al., 1992b). ^{15}N decoupling is optional and can be applied in order to remove unresolved two-bond and three-bond ^{15}N,$^1H^{\alpha}$ couplings from the $^1H^{\alpha}$ resonances.

The spectrum was recorded as a 128 (complex) × 32 (complex) × 1024 (real) data set with acquisition times of 85.5, 10.3 and 106.5 ms in t_1, t_2 and t_3, respectively. Spectral widths in F1, F2 and F3 comprised 1488, 3012 and 4808 Hz. The size of the real part of the 3D spectrum was 512 (F1) × 64 (F2) × 1024 (F3). The total measuring time, using 16 scans per increment, was 91 h.

All spectra were processed on Silicon Graphics workstations with the FELIX program (version 1.1; Hare Research, Inc.). After Fourier transformation in the t_3 dimension, linear prediction was employed to extend the time-domain data by approximately 33% in the ^{15}N dimensions of all spectra and in the $^{13}C^{\alpha}$ dimensions of the spectra recorded with pulse sequences A, C, D and F. Squared sine-bell weighting functions shifted by $\pi/5$–$\pi/2$ were used for apodization in all dimensions. For the

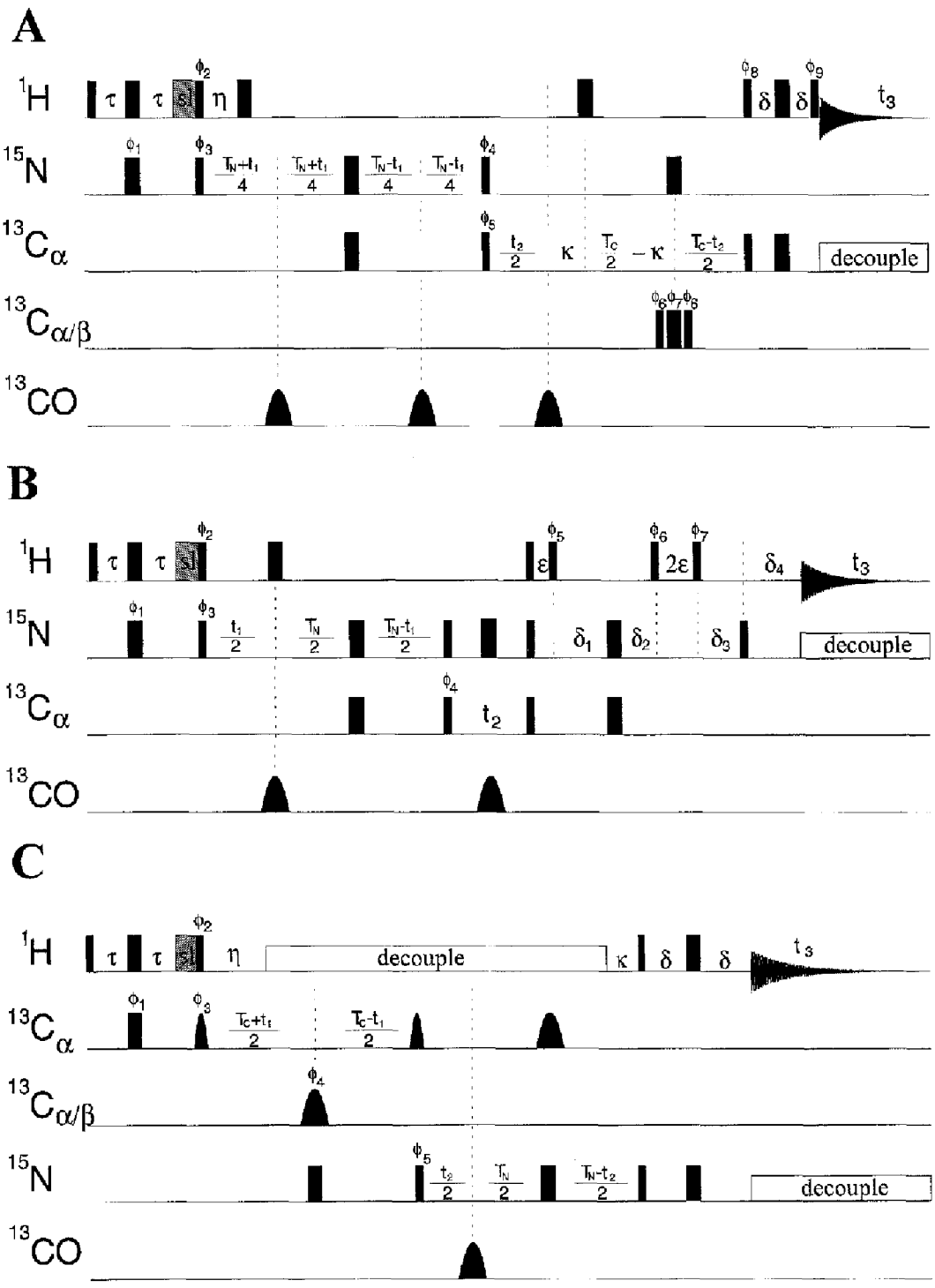

Fig. 2. Pulse schemes for the measurement of $^{3}J_{HNH^{\alpha}}$ (A,B,C), $^{3}J_{HNCO}$ (C,D), $^{3}J_{HNC\beta}$ (E) and $^{3}J_{H^{\alpha}CO}$ (F) coupling constants. Narrow and wide rectangles denote 90° and 180° pulses, respectively. Rectangular pulses on $^{13}C^{\alpha}$ nuclei are applied at 60 ppm (A,B,E,F) or at 58 ppm (C,D) with an rf field strength of 4.63 kHz. The 180° pulses on aliphatic carbons during the $^{13}C^{\alpha}$ constant-time evolution periods are centered at 45 ppm. In scheme A, a composite pulse with a field strength of 5.17 kHz is applied to the $^{13}C^{\alpha/\beta}$ region, whereas G3 pulses with a duration of 256 μs are used in the pulse sequences C, D and F. Band-selective excitation and inversion of $^{13}C^{\alpha}$ spins is achieved with Gaussian cascades G4 and G3. Every other carbon 90° pulse has a time-reversed G4 shape. Pulse widths are 768 and 512 μs for 90° and 180° flip angles, respectively, in sequences C, D and F or 2.05 and 1.28 ms in the case of sequence E. Carbonyl 180° pulses are implemented as phase-modulated pulses with an amplitude profile corresponding to the central lobe of a sinc function and a duration of 108 μs. The proton carrier is placed on the H_2O resonance frequency throughout sequences A, B and F, whereas it is shifted in the remaining experiments to the centre of the amide region (8.6 ppm) subsequent to pulses labeled ϕ_2. Water suppression is achieved by weak presaturation during the relaxation delay and spin-lock purge pulses (sl) with a duration of 2 ms, except for the first spin-lock pulse in sequence F which is applied for 3 ms. Proton decoupling is accomplished by WALTZ-16 modulation (Shaka et al., 1983) with a 5 kHz rf field. The GARP-1 sequence (Shaka et al., 1985) is used for ^{15}N-decoupling during acquisition with a field strength of 1.1 kHz and for ^{13}C-decoupling in scheme A with a field strength of 1.5 kHz. Band-selective decoupling of $^{13}C^{\alpha}$ resonances in scheme

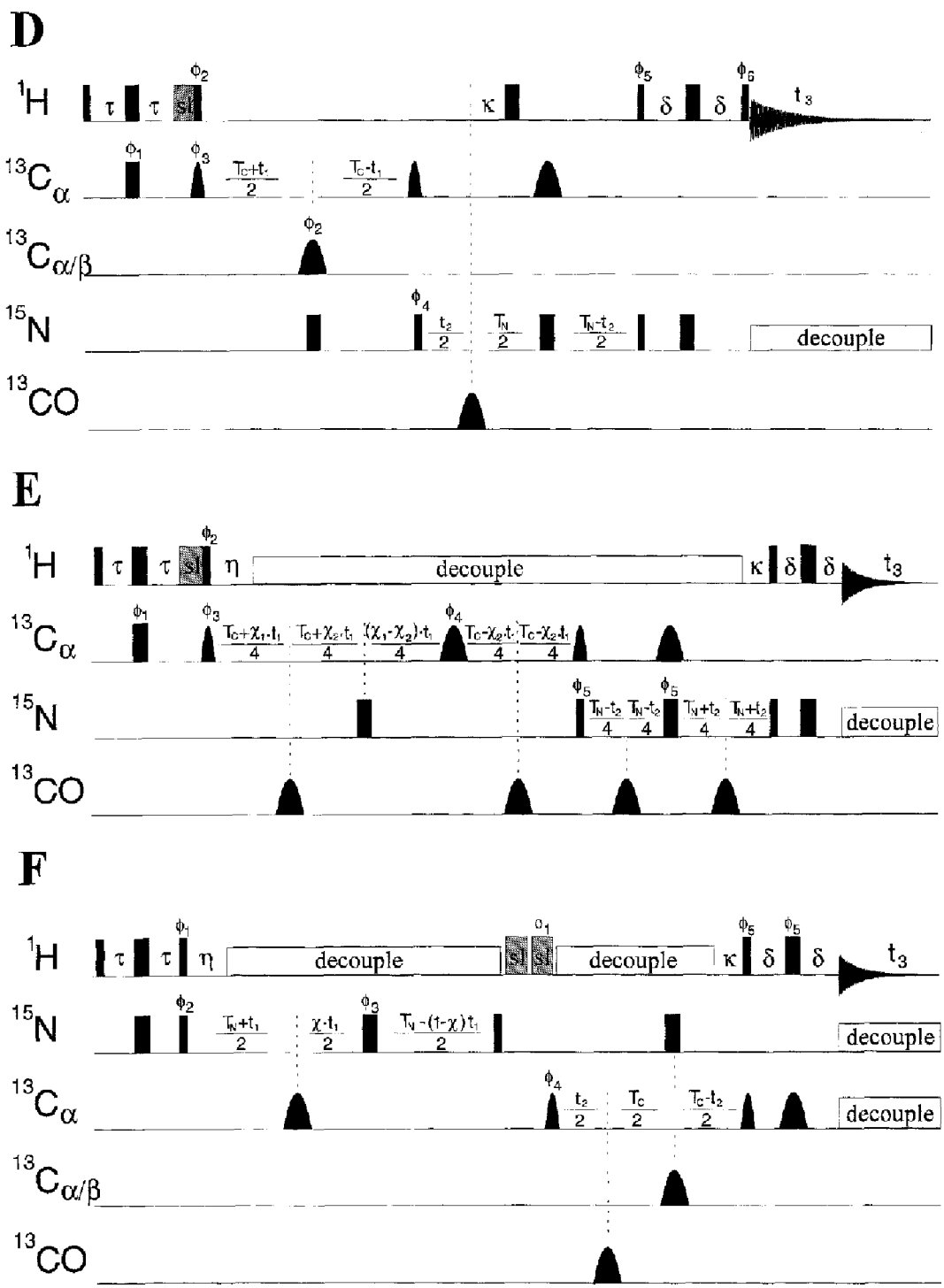

F is achieved using an MLEV-16 expansion of a 768 μs G3 pulse cascade. Delay durations and phase cycles are: (A) $\tau = 2.3$ ms, $\eta = 2.75$ ms, $T_N = 22$ ms, $T_C = 26.6$ ms, $\kappa = 0.95$ ms, $\delta = 1.4$ ms, $\phi_1 = 2(x),2(-x)$, $\phi_2 = 2(y),2(-y)$, $\phi_3 = 4(x),4(-x)$, $\phi_4 = 16(x),16(-x)$, $\phi_5 = 8(x),8(-x)$, $\phi_6 = 16(x),16(y)$, $\phi_7 = 16(y),16(-x)$, $\phi_8 = x,-x$, $\phi_9 = -x,x$, rec.: +,−,−,+,−,+,+,−,−,+,+,−,+,−,−,+; (B) $\tau = 2.3$ ms, $T_N = 22$ ms, $\varepsilon = 65$ μs, $\delta_1 = 10.04$ ms, $\delta_2 = 2.2$ ms, $\delta_3 = 7.775$ ms, $\delta_4 = 4.465$ ms + $\tau_{180°}$ ($^{13}C^{\alpha}$) − $\tau_{90°}$(^{15}N), where $\tau_{180°}$ ($^{13}C^{\alpha}$) and $\tau_{90°}$ (^{15}N) are the pulse widths of 180° ($^{13}C^{\alpha}$) and 90° (^{15}N) pulses, respectively, $\phi_1 = x,-x$, $\phi_2 = y,-y$, $\phi_3 = 2(x),2(-x)$, $\phi_4 = 4(x),4(-x)$, $\phi_5 = -x$, $\phi_6 = 8(x),8(y),8(-x),8(-y)$, $\phi_7 = 8(-x),8(-y),8(x),8(y)$, rec.: +,−,−,+,−,+,+,−,−,+,+,−,+,−,−,+; (C) $\tau = 1.7$ ms, $\eta = 2$ ms, $T_C = 26.6$ ms, $T_N = 22$ ms, $\kappa = 5$ ms, $\delta = 2.3$ ms, $\phi_1 = x,-x$, $\phi_2 = y,-y$, $\phi_3 = 2(x),2(-x)$, $\phi_4 = 8(y),8(-y)$, $\phi_5 = 4(x),4(-x)$, rec.: +,−,−,+,−,+,+,−; (D) $\tau = 1.7$ ms, $T_C = 26.6$ ms, $T_N = 22$ ms, $\kappa = 2.5$ ms, $\phi_1 = x,-x$, $\phi_2 = y,-y$, $\phi_3 = 2(x),2(-x)$, $\phi_4 = 8(x),8(-x)$, $\phi_5 = 4(x),4(-x)$, $\phi_6 = 4(-x),4(x)$, rec.: +,−,−,+,−,+,+,−,−,+,+,−,−,+; (E) $\tau = 1.7$ ms, $\eta = 3.4$ ms, $T_C = 30$ ms, $\chi^1 = 1.44$, $\chi^2 = 2-\chi^1$, $T_N = 22$ ms, $\kappa = 5.5$ ms, $\delta = 2.3$ ms, $\phi_1 = x,-x$, $\phi_2 = y,-y$, $\phi_3 = 2(x),2(-x)$, $\phi_4 = 8(x),8(-x)$, $\phi_5 = 4(x),4(-x)$, rec.: +,−,−,+,−,+,+,−; (F) $\tau = 2.3$ ms, $\eta = 5.4$ ms, $T_N = 31$ ms, $\chi = 0.64$, $T_C = 26.6$ ms, $\kappa = 2.1$ ms, $\delta = 1.7$ ms, $\phi_1 = y$, $\phi_2 = 2(x),2(-x)$, $\phi_3 = 8(x),8(-x)$, $\phi_4 = 4(x),4(-x)$, $o_5 = x,-x$, rec.: +,−,−,+,−,+,+,−. Nonlabeled pulses are applied along the x-axis. Quadrature detection in the t_1 and t_2 dimensions is obtained by altering the phases ϕ_3 and ϕ_5 (A,C,E), ϕ_3 and ϕ_4 (B,D), and ϕ_2 and ϕ_4 (F) in a TPPI (Marion and Wüthrich, 1983) or States-TPPI manner (Marion et al., 1989).

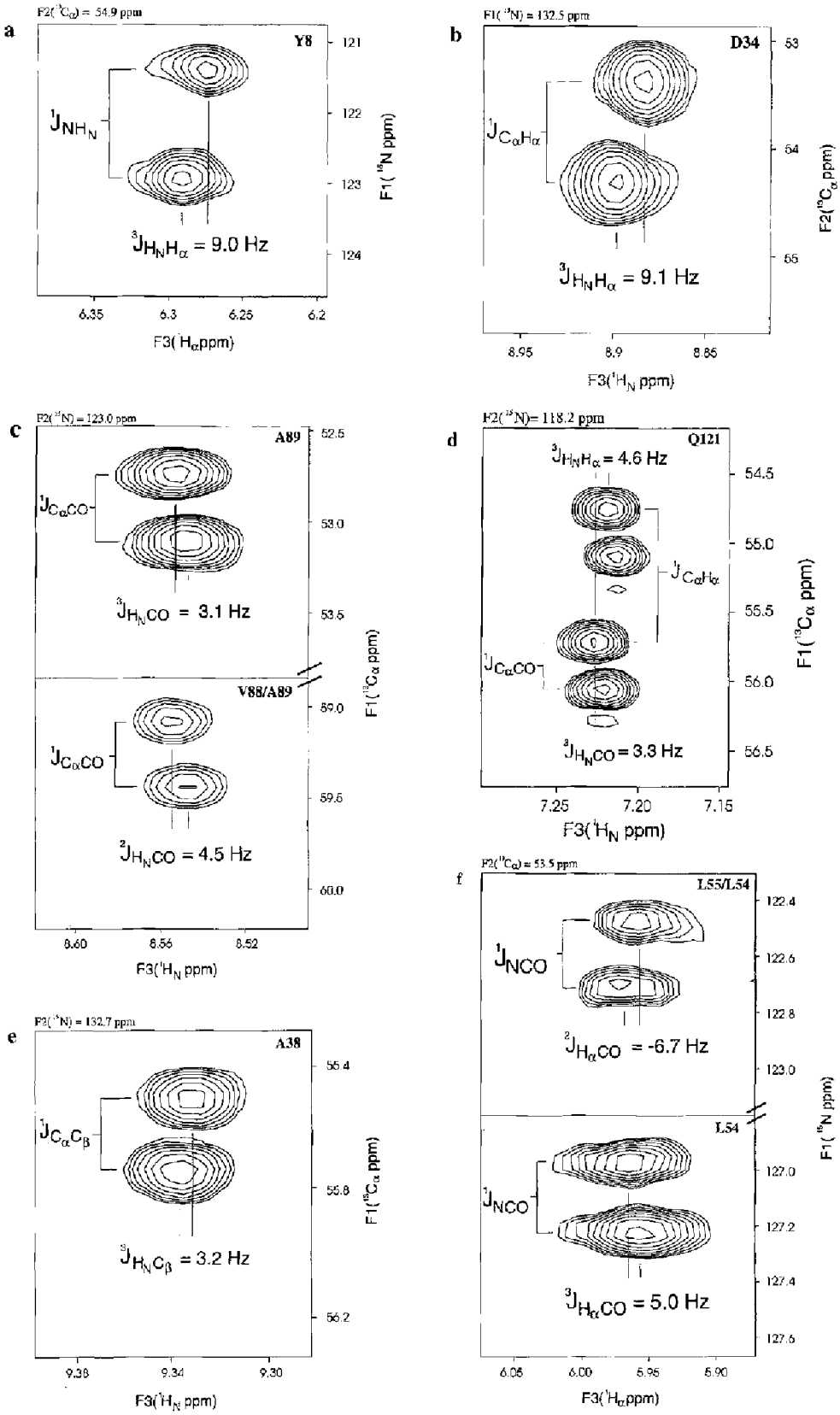

Fig. 3. Application of the pulse sequences depicted in Fig. 2 to uniformly $^{13}C/^{15}N$-labeled oxidized *D. vulgaris* flavodoxin. Panels a–f show expansions of F1,F3 or F2,F3 slices from the 3D spectra obtained with the experimental schemes labeled with the corresponding capital letters. The cross peaks exhibit an E.COSY-type multiplet pattern with a large splitting along F1 or F2, due to one-bond couplings, and a small displacement along F3 due to three-bond couplings for intraresidual correlations and two-bond couplings for the shown interresidual correlations. Assignments as well as measured vicinal and geminal coupling constants are indicated. In panel d positive and negative levels are plotted without distinction.

extraction of vicinal and geminal coupling constants from the 3D data sets, two F3 traces, corresponding to the upper and lower E.COSY multiplet component, were generated by summing over the spectral points in F1 and F2. Inverse Fourier transformation, followed by zero-filling, yielded digital resolutions between 0.27 and 0.29 Hz/point. Subsequently, the F3 traces were subtracted and the displacement was determined from the difference spectra by calculating the power integrals as a function of incremented frequency shifts (Schwalbe et al., 1993).

Results and Discussion

The application of pulse sequences A–F to $^{13}C/^{15}N$-doubly labeled proteins leads to heteronuclear E.COSY cross peaks from which $^3J_{H^N H^\alpha}$, $^3J_{H^N CO}$, $^3J_{H^N C^\beta}$ or $^3J_{H^\alpha CO}$ coupling constants can be determined. As an example, pulse sequence A will be described in terms of the product operator formalism (Sørensen et al., 1983) without considering relaxation effects. For simplicity, only terms that result in observable magnetization during the detection period t_3 are retained and nonrelevant $^1H,^1H$, $^1H,^{13}C$ and $^1H,^{15}N$ couplings are not included. The spin operators $\mathbf{H}^N$, $\mathbf{H}^\alpha$, $\mathbf{N}$ and $\mathbf{C}^\alpha$ denote magnetization components of the $^1H^N$, $^1H^\alpha$, ^{15}N and $^{13}C^\alpha$ nuclei, respectively.

The initial INEPT transfer (Morris and Freeman, 1979) converts longitudinal amide proton magnetization ($\sigma(0) = \mathbf{H}_z^N$) into antiphase ^{15}N magnetization according to:

$$\sigma(2\tau) = -2\mathbf{H}_z^N \mathbf{N}_y \sin(2\pi\, {}^1J_{NH^N}\tau) \qquad (1)$$

During the constant-time ^{15}N evolution period T_N, the ^{15}N-$^{13}C^\alpha$ coupling leads to dephasing of the $\mathbf{H}_z^N\mathbf{H}_y$ term while the effects of the $^{15}N/^{13}CO$ scalar interaction are refocused by the ^{13}CO-selective 180° pulses. ^{15}N chemical shift and $^1J_{NH^N}$ evolution take place as a function of t_1. Considering only intraresidual correlations, these processes are described by:

$$\begin{aligned}\sigma(2\tau,T_N) = [&-4\mathbf{H}_z^N\mathbf{N}_y\mathbf{C}_z^\alpha \sin(\Omega_N t_1)\sin(\pi\, {}^1J_{NH^N}t_1)\\ &+ 2\mathbf{N}_y\mathbf{C}_z^\alpha \cos(\Omega_N t_1)\cos(\pi\, {}^1J_{NH^N}t_1)]\\ \times \sin(2\pi\, {}^1J_{NH^N}\eta)&\sin(\pi\, {}^1J_{NC^\alpha}T_N)\cos(\pi\, {}^2J_{NC^\alpha}T_N)\end{aligned} \qquad (2)$$

where Ω_N is the ^{15}N angular frequency and η is set to $1/(4\, {}^1J_{NH^N})$. The pair of simultaneous 90° $^{13}C^\alpha/^{15}N$ pulses converts the ^{15}N antiphase magnetization into ^{13}C antiphase magnetization. In the subsequent constant-time $^{13}C^\alpha$ chemical-shift evolution period T_C, $^{13}C^\alpha$ antiphase magnetization is refocused with respect to amide nitrogens. Again, the effect of J-coupling to carbonyl carbons is eliminated by applying a shaped 180° ^{13}CO pulse at time $t_2/2$, whereas the $^1J_{C^\alpha C^\beta}$ coupling is active throughout T_C. $^{13}C^\alpha$ antiphase magnetization with respect to the α-proton(s) builds up for a duration of 2κ. These effects can be summarized as follows:

$$\begin{aligned}\sigma(2\tau,T_N,T_C) = [&4\mathbf{H}_z^N\mathbf{H}_z^\alpha\mathbf{C}_y^\alpha \sin(\Omega_N t_1)\sin(\pi\, {}^1J_{NH^N}t_1)\\ &+ 2\mathbf{H}_z^\alpha\mathbf{C}_y^\alpha \cos(\Omega_N t_1)\cos(\pi\, {}^1J_{NH^N}t_1)]\\ \cos(\Omega_{C^\alpha}t_2)&\sin(\pi\, {}^1J_{NC^\alpha}T_C)\cos(\pi\, {}^2J_{NC^\alpha}T_C)\\ \sin(2\pi\, {}^1J_{C^\alpha H^\alpha}\kappa)&\cos^n(2\pi\, {}^1J_{C^\alpha H^\alpha}\kappa)\cos(\pi\, {}^1J_{C^\alpha C^\beta}T_C)\end{aligned} \qquad (3)$$

where the exponent n is 1 for glycine and 0 for all other residues. The duration T_C has to be adjusted to $1/{}^1J_{C^\alpha C^\beta}$ (i.e., approximately 27 ms) in order to remove the effect of the $^{13}C^\alpha$-$^{13}C^\beta$ scalar coupling. The final reverse INEPT sequence creates detectable transverse magnetization of α-protons given by:

$$\begin{aligned}(2\tau,T_N,T_C,2\delta) = [&2\mathbf{H}_z^N\mathbf{H}_x^\alpha \sin(\Omega_N t_1)\sin(\pi\, {}^1J_{NH^N}t_1)\\ &+ \mathbf{H}_x^\alpha \cos(\Omega_N t_1)\cos(\pi\, {}^1J_{NH^N}t_1)]\\ &\times \cos(\Omega_{C^\alpha}t_2)\sin(2\pi\, {}^1J_{C^\alpha H^\alpha}\delta)\end{aligned} \qquad (4)$$

The superposition of the two terms detected during t_3 results in an E.COSY-type cross peak with an in-phase splitting due to $^1J_{NH^N}$ along F1 and $^3J_{H^N H^\alpha}$ along F3. The signal amplitude is given by:

$$\begin{aligned}\sigma(t_1,t_2,t_3) = \mathbf{H}_x^\alpha &\cos(\Omega_{C^\alpha}t_2)\\ [\sin(\Omega_N t_1)\sin(\pi\, {}^1J_{NH^N}t_1)&\sin(\Omega_{H^\alpha}t_3)\sin(\pi\, {}^3J_{H^N H^\alpha}t_3)\\ + \cos(\Omega_N t_1)\cos(\pi\, {}^1J_{NH^N}t_1)&\cos(\Omega_{H^\alpha}t_3)\cos(\pi\, {}^3J_{H^N H^\alpha}t_3)]\end{aligned} \qquad (5A)$$

where constant multiplicative factors that result from the magnetization transfer steps have been excluded. For pulse sequences B–F the respective expressions are:

$$\begin{aligned}\sigma(t_1,t_2,t_3) = \mathbf{H}_x^N &\cos(\Omega_N t_1)\\ [\sin(\Omega_{C^\alpha}t_2)\sin(\pi\, {}^1J_{C^\alpha H^\alpha}t_2)&\sin(\Omega_{H^N}t_3)\sin(\pi\, {}^3J_{H^N H^\alpha}t_3)\\ + \cos(\Omega_{C^\alpha}t_2)\cos(\pi\, {}^1J_{C^\alpha H^\alpha}t_2)&\cos(\Omega_{H^N}t_3)\cos(\pi\, {}^3J_{H^N H^\alpha}t_3)]\end{aligned} \qquad (5B)$$

$$\begin{aligned}\sigma(t_1,t_2,t_3) = \mathbf{H}_x^N &\cos(\Omega_N t_2)\\ [\sin(\Omega_{C^\alpha}t_1)\sin(\pi\, {}^1J_{C^\alpha CO}t_1)&\sin(\Omega_{H^N}t_3)\sin(\pi\, {}^3J_{H^N CO}t_3)\\ + \cos(\Omega_{C^\alpha}t_1)\cos(\pi\, {}^1J_{C^\alpha CO}t_1)&\cos(\Omega_{H^N}t_3)\cos(\pi\, {}^3J_{H^N CO}t_3)]\end{aligned} \qquad (5C)$$

$$\begin{aligned}\sigma(t_1,t_2,t_3) = \mathbf{H}_x^N &\cos(\Omega_N t_2)\\ [&\sin(\Omega_{C^\alpha}t_1)\sin(\pi\, {}^1J_{C^\alpha H^\alpha}t_1)\cos(\pi\, {}^1J_{C^\alpha CO}t_1)\\ &\cos(\Omega_{H^N}t_3)\cos(\pi\, {}^3J_{H^N H^\alpha}t_3)\cos(\pi\, {}^3J_{H^N CO}t_3)\\ +\ &\sin(\Omega_{C^\alpha}t_1)\sin(\pi\, {}^1J_{C^\alpha H^\alpha}t_1)\sin(\pi\, {}^1J_{C^\alpha CO}t_1)\\ &\sin(\Omega_{H^N}t_3)\cos(\pi\, {}^3J_{H^N H^\alpha}t_3)\sin(\pi\, {}^3J_{H^N CO}t_3)\\ +\ &\cos(\Omega_{C^\alpha}t_1)\cos(\pi\, {}^1J_{C^\alpha H^\alpha}t_1)\cos(\pi\, {}^1J_{C^\alpha CO}t_1)\\ &\sin(\Omega_{H^N}t_3)\sin(\pi\, {}^3J_{H^N H^\alpha}t_3)\cos(\pi\, {}^3J_{H^N CO}t_3)\\ +\ &\sin(\Omega_{C^\alpha}t_1)\cos(\pi\, {}^1J_{C^\alpha H^\alpha}t_1)\sin(\pi\, {}^1J_{C^\alpha CO}t_1)\\ &\cos(\Omega_{H^N}t_3)\sin(\pi\, {}^3J_{H^N H^\alpha}t_3)\sin(\pi\, {}^3J_{H^N CO}t_3)]\end{aligned} \qquad (5D)$$

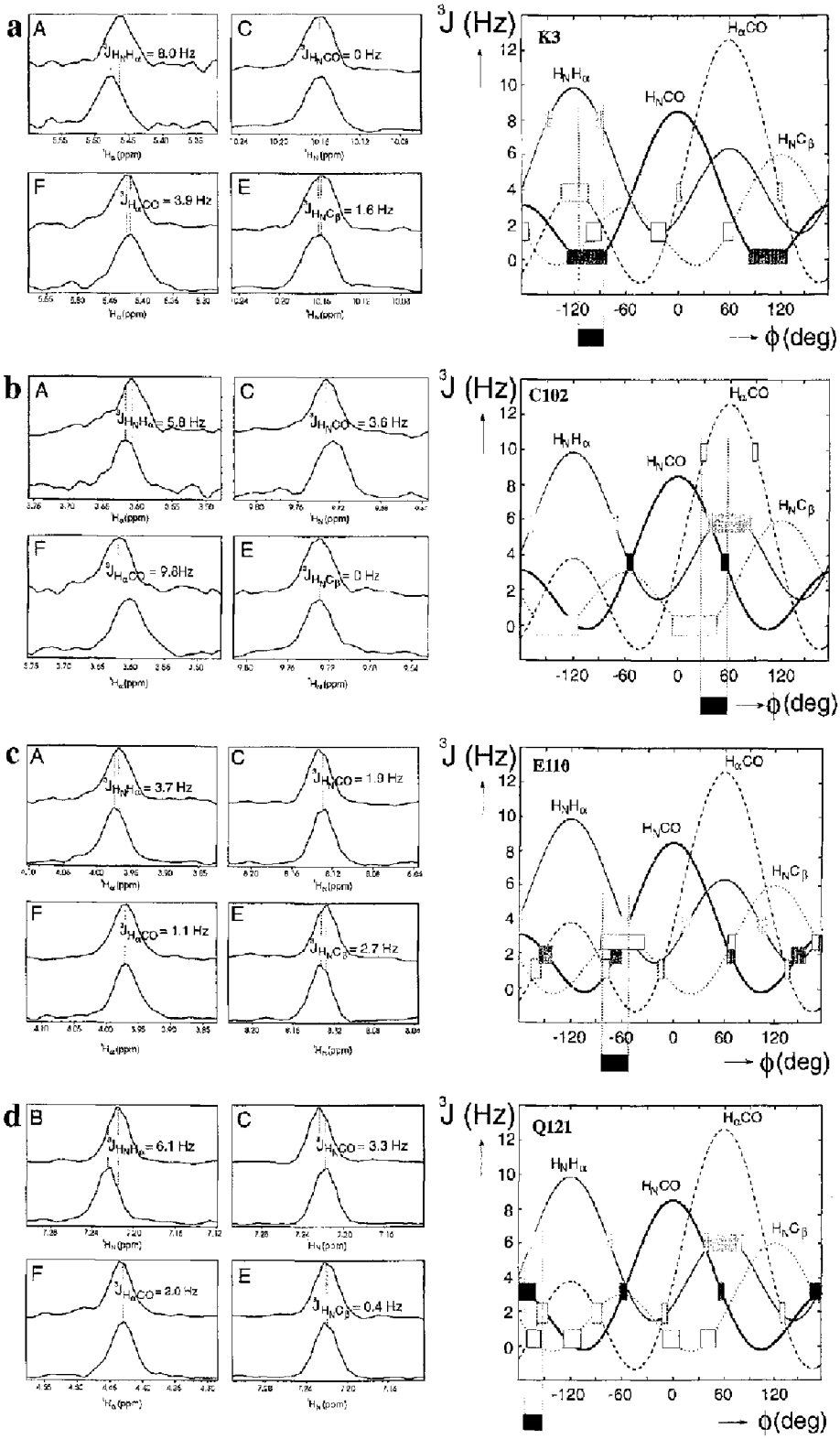

Fig. 4. Left: values of $^3J_{HNH\alpha}$, $^3J_{HNCO}$, $^3J_{HNC\beta}$ and $^3J_{H\alpha CO}$ determined for residues (a) Lys[3]; (b) Cys[102]; (c) Glu[110]; and (d) Gln[121] of *D. vulgaris* flavodoxin. The cross sections of the upper and lower multiplet components along F3 were obtained by summation over appropriate slices in F1 and F2 in the spectra recorded with the pulse sequences marked in the upper left corner of the expansions. To increase digital resolution, the rows were inverse Fourier transformed, zero-filled to 16K complex points and Fourier transformed again. Right: Karplus curves for the measured coupling constants with parameters taken from Vuister and Bax (1993) for $^3J_{HNH\alpha}$, from Bystrov et al. (1975) for $^3J_{H\alpha CO}$ and from Bystrov (1976) for $^3J_{HNCO}$ and $^3J_{HNC\beta}$. The ϕ-angle ranges that correspond to the measured vicinal couplings, assuming an uncertainty of ±0.5 Hz, are indicated by open and hatched rectangles. The filled rectangles denote the most probable ϕ-angle ranges as judged by the coincidence of the individual regions.

$$\sigma(t_1,t_2,t_3)= H_x^N \cos(\Omega_N t_2) \quad (5E)$$
$$[\sin(\Omega_{C\alpha}t_1)\sin(\pi\ ^1J_{C\alpha C\beta}t_1)\sin(\Omega_{H^N}t_3)\sin(\pi\ ^3J_{H^NC\beta}t_3)$$
$$+\cos(\Omega_{C\alpha}t_1)\cos(\pi\ ^1J_{C\alpha C\beta}t_1)\cos(\Omega_{H^N}t_3)\cos(\pi\ ^3J_{H^NC\beta}t_3)]$$

$$\sigma(t_1,t_2,t_3)= H_x^\alpha \cos(\Omega_{C\alpha}t_2) \quad (5F)$$
$$[\sin(\Omega_N t_1)\sin(\pi\ ^1J_{NCO}t_1)\sin(\Omega_{H\alpha}t_3)\sin(\pi\ ^3J_{H\alpha CO}t_3)$$
$$+\cos(\Omega_N t_1)\cos(\pi\ ^1J_{NCO}t_1)\cos(\Omega_{H\alpha}t_3)\cos(\pi\ ^3J_{H\alpha CO}t_3)]$$

The proposed pulse sequences yield the coupling constant information required for the determination of the backbone torsion angle ϕ in proteins. In the F1–F3 planes of the 3D spectra the cross peaks exhibit the desired E.COSY multiplet patterns, as demonstrated in Fig. 3. The experiments were performed using a uniformly $^{13}C/^{15}N$-labeled sample of oxidized flavodoxin from *Desulfovibrio vulgaris*, a flavoprotein consisting of 147 amino acids and equimolar noncovalently bound FMN (for a review see Mayhew and Tollin (1992)).

All vicinal couplings that could be extracted from cross peaks shown in Fig. 3 have the same relative sign. The reverse tilt observed in panels e, d and f is due to the fact that complementary E.COSY patterns are obtained when an odd number of inversion pulses is applied to the passive spin. Here, a 180° pulse on carbonyl carbons had to be inserted in order to refocus the $^1J_{NCO}$ and the $^1J_{C\alpha CO}$ couplings in the F2 dimensions of the (H)CANNH and (H)NCAHA experiments, respectively.

For the sequential connectivities in the spectra with pulse sequences C, D and F, the displacement of the upper and lower submultiplets is caused by geminal $^1H,^{13}C$ couplings. The $^2J_{H\alpha CO}$ coupling may be useful, because it correlates with the backbone torsion angle ψ (Hansen, 1991). However, $^2J_{H\alpha CO}$ as well as $^2J_{HNCO}$ can be obtained with higher sensitivity from HSQC experiments (Delaglio et al., 1991; Vuister and Bax, 1992; Madsen et al., 1993) and are just a by-product of the pulse sequences presented here.

An obvious disadvantage of the experiments which detect α-protons during t_3 is the fact that no coupling constants can be evaluated when the $^1H^\alpha$ resonances are located near the strong residual H_2O signal. Therefore, we also recorded an HNCA-type experiment (B) for determining $^3J_{HNH\alpha}$. As pointed out by Görlach et al. (1993), protein $^1H^\alpha$ spin flips, caused by dipolar relaxation between the $^{13}C^\alpha$ evolution period and the detection of amide protons, lead to a significant attenuation of one of the two branches contributing to the observed cross peaks. In the resulting corrupted E.COSY patterns the peak maxima are shifted towards the centre of the cross peaks along F3 and the $^3J_{HNH\alpha}$ coupling constants tend to be underestimated. To account for these effects, nitrogen antiphase magnetization with respect to amide protons can be converted into ^1H-^{15}N multiple-quantum coherence during the back-transfer of coherence from $^{13}C^\alpha$ to the amide protons. In the pulse schemes introduced by Gör-

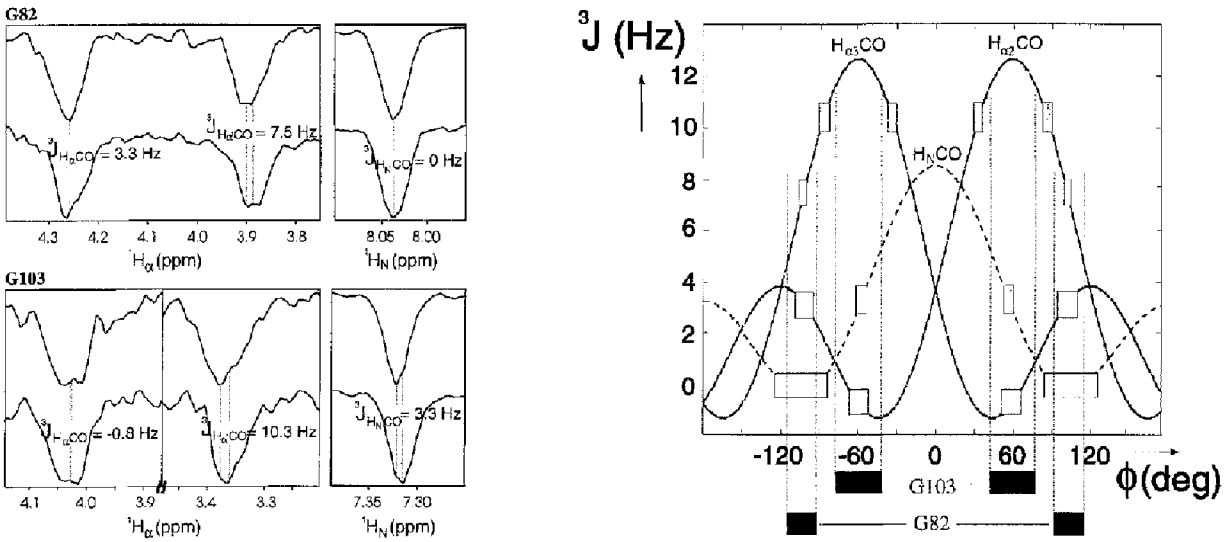

Fig. 5. Determination of possible ϕ-angle ranges for two glycine residues of *D. vulgaris* flavodoxin. The $^3J_{H\alpha CO}$, $^3J_{H\alpha'CO}$ and $^3J_{HNCO}$ coupling constants for Gly^{82} (top left) and Gly^{103} (bottom left) were extracted from a CO-coupled (H)NCAHA and a CO-coupled (H)CANNH spectrum, recorded with the pulse sequences F and C, respectively. The reversed sign of the signals is due to the absence of the C^α, C^β coupling effect (factor $\cos[\pi\ ^1J(C^\alpha C^\beta)T_C]$) in the transfer functions for glycine residues. H^α and $H^{\alpha'}$ denote the low-field and up-field α-proton resonances, respectively. Note that the F3 cross sections through the upper and lower submultiplets are plotted with different scales for the $^1H^\alpha$ and the $^1H^N$ domains. At the right the Karplus curves for the $^1H^{\alpha 2},^{13}CO$, $^1H^{\alpha 3},^{13}CO$ and $^1H^N,^{13}CO$ vicinal couplings are shown together with ϕ-angle ranges that correspond to the experimental values, arbitrarily assuming an uncertainty of ±0.5 Hz. Open boxes are used for Gly^{82} and hatched boxes for Gly^{103}. Torsion angles that can be excluded by combination of the coupling constant information are not indicated. In the case of Gly^{103}, the value obtained for $^3J_{H\alpha'CO}$ does not exactly match the region suggested by the two remaining couplings. This might be due to an experimental error larger than ±0.5 Hz. Note that the drawn Karplus curves represent only the centre of an allowed region. Two possible ϕ-angle ranges, symmetric about ϕ = 0, can be assigned for each glycine residue.

TABLE 1
VICINAL COUPLING CONSTANTS (Hz) DETERMINED FOR OXIDIZED *D. vulgaris* FLAVODOXIN

Residue	$^3J_{HNH\alpha}$[a]	$^3J_{HNCO}$[b]	$^3J_{HN C\beta}$	$^3J_{H\alpha CO}$	Secondary structure
Lys[3]	8	0	1.6	3.9	s
Ile[6]	8.1	0.6	1.2	–	s
Tyr[8]	9	0.6	–0.8	2.4	s
Ser[10]	6.2	1.6	–	2.6	
Thr[11]	7.8	0	–	2.5	
Glu[16]	4.6	0.9	2.9	0.7	h
Tyr[17]	–	1.7	2.6	0.5	h
Ala[19]	3.5	1.7	3.3	0.5	h
Ile[22]	–	0.8	3.1	0.8	h
Ala[23]	3.7	2.3	3.1	1.3	h
Arg[24]	3.3	1.4	2.5	1.1	h
Leu[26]	4.2	0.8	1.7	2.1	h
Asp[28]	3.9	2	2.3	–	h
Ala[29]	8.6	0.3	–	2.7	
Tyr[31]	6.4	–0.3	1.8	–	
Glu[32]	8.8	–0.2	1.7	–	s
Val[33]	8.6	0	0.5	–	s
Asp[34]	9.1	–0.4	1.5	–	s
Ser[35]	9.7	0.2	–	4.3	s
Arg[36]	8.9	0.9	–0.2	–	s
Asp[37]	5.7	0.2	2.8	1.7	
Ala[38]	2.7	2.6	3.2	–	
Ser[40]	8.6	0	–	3	
Val[41]	8.9	0.5	0.4	–	
Glu[42]	9.5	0.9	0.8	2.6	
Ala[43]	3.8	2	3.1	0.9	
Phe[47]	6.2	0	2.2	–	
Glu[48]	2.8	1.4	2.6	0.8	
Phe[50]	6.7	0.2	2.5	2.4	
Val[53]	8.9	0	0.2	–	s
Leu[54]	9.2	0.9	–	5	s
Trp[60]	7.1	1.2	–0.8	4.4	
Ser[64]	6.7	2.3	–	1.5	
Ile[65]	3.7	0.5	2.2	1.1	
Leu[67]	–	0.2	1.7	1.5	
Asp[70]	5.6	0.5	2	2.2	h
Leu[74]	–	0.3	2.5	0.2	h
Phe[75]	–	1.5	2.8	0	h
Asp[76]	3.8	1.4	2.5	0.6	h
Glu[79]	4.8	1.7	2	0.7	h
Gln[84]	2.6	1.2	3	–0.7	
Arg[86]	8.3	–0.2	1.7	2.7	
Lys[87]	5.8	0	2.6	–	
Val[88]	–	1.1	0	2.9	s
Ala[89]	5.4	3.1	0.2	–	s
Cys[90]	9.5	0.4	–	3.4	s
Phe[91]	7.7	1.2	0	1.7	s
Glu[99]	3	–	2.2	1.1	
Phe[101]	2	1.2	2	–	
Cys[102]	5.8	3.6	0	9.8	
Asp[106]	2.8	1.5	2.6	0.2	h
Ala[107]	4.1	1.6	3.2	1.7	h
Ile[108]	4.7	1.1	–	1.4	h
Glu[109]	–	1.5	2.8	0.6	h
Glu[110]	3.7	1.9	2.7	1.1	h
Leu[112]	–	1.1	3.1	1.1	h
Lys[113]	3.4	1.4	2.8	–	h
Asn[114]	4.5	0.9	2.6	1.7	h
Leu[115]	6.1	0.1	1.9	2.2	
Ala[117]	5.9	0.6	3.1	–	
Ile[119]	6.9	0.2	2.8	–	
Val[120]	5.6	1.3	2.6	3.6	
Gln[121]	6.1	3.3	0.4	2	

TABLE 1
(continued)

Residue	$^3J_{HNH\alpha}$[a]	$^3J_{HNCO}$[b]	$^3J_{HNC\beta}$	$^3J_{H\alpha CO}$	Secondary structure
Asp[122]	4.6	1.5	2.5	–	
Leu[124]	6.7	1.2	1.7	2.7	s
Ile[126]	7.8	–0.5	1.3	2.7	s
Asp[129]	3.7	0.9	2.8	–	
Arg[131]	3.9	1.2	–	1.7	
Ala[132]	7.3	0.1	–	1.6	
Asp[135]	3.6	0.8	2.1	–	h
Ile[137]	4.1	0.8	2.9	–	h
Val[138]	4.4	1.4	3.9	1.7	h
Trp[140]	3.9	0.9	3.3	–	h
Ala[141]	4.7	1.4	2.9	1.4	h
His[142]	4	1.5	3.3	0.8	h
Asp[143]	4.8	0.9	2.7	2	h
Val[144]	3.9	1.4	3	1.5	h
Arg[145]	3.1	1.7	2.8	–	h
Ile[148]	8.4	0.5	1.1	2.6	

Only residues for which values of more than two different couplings could be obtained are listed. Helical segments (h) and β-strands (s), as identified by NOE contacts (Knauf et al., 1993), are indicated in the right column.

[a] From either experiment A or B.

[b] From experiment C.

lach et al. (1993), shaped band-selective pulses on amide protons are employed to avoid perturbation of $^1H^\alpha$ spins and to refocus the passive $^1H^N$,$^1H^\alpha$ coupling during the persistence of the proton–nitrogen multiple-quantum coherence. Since we only used the HNCA-type experiment as a supplement to the (H)NCAHA experiment A for amino acid residues with $^1H^\alpha$ chemical shifts in the vicinity of the H_2O resonance, the 1-1 echo sequence (Sklenář and Bax, 1987) was implemented for the same purpose. This variant considerably facilitated water suppression.

No effort was made to minimize the influence of the above-mentioned relaxation effects in the CO,H^α-coupled (H)CANNH experiment D. As a consequence, the measured $^3J_{HNH\alpha}$ coupling constants were generally smaller than those extracted from experiments A and B for the same residues. A vicinal $^1H^N$,$^1H^\alpha$ coupling constant of 4.6 Hz was obtained for Gln[121] (see Fig. 3d), whereas a value of 6.1 Hz was measured in the spectrum recorded with pulse sequence B (Fig. 4d). The simultaneous determination of two different coupling constants from E.COSY patterns that are split into four submultiplets is possible, although with reduced sensitivity (Eggenberger et al., 1992a). The signal-to-noise ratio in two separate experiments is higher by a factor of $2^{1/2}$ when compared to an experiment with two passive splittings, acquired in the same measuring time.

The combined use of $^3J_{HNH\alpha}$, $^3J_{HNCO}$, $^3J_{HNC\beta}$ and $^3J_{H\alpha CO}$ coupling constants is demonstrated in Fig. 4 for selected residues of flavodoxin. In all cases the values for one vicinal coupling correspond to several conformations about the ϕ-torsion angle according to the Karplus equations. If all available three-bond couplings are considered, only one possibility remains under the assumption of a single rigid conformation. In particular, for Cys[102] the positive ϕ-angle would not have been detected using the $^1H^N$,$^1H^\alpha$ coupling constant only. The relatively high values for both $^3J_{HNCO}$ and $^3J_{H\alpha CO}$ exclude local conformations with a negative ϕ-angle.

Among the 147 amino acid residues of flavodoxin, 18 are glycines and three are prolines. From the spectra recorded with pulse sequences A and B, 89 $^3J_{HNH\alpha}$ coupling constants could be extracted for the remaining residues. Evaluation of cross peaks in the CO-coupled (H)CANNH (C), the C^β-coupled (H)CANNH (E) and the CO-coupled (H)NCAHA (F) spectra resulted in the determination of 98 $^3J_{HNCO}$, 79 $^3J_{HNC\beta}$ and 62 $^3J_{H\alpha CO}$ values. Table 1 summarizes the measured coupling constants for those residues where experimental data for at least three couplings were available.

The situation encountered for glycine residues is less clear. Constraints for the ϕ-angle cannot be obtained solely by use of coupling constants. The H^N- and CO-coupled (H)NCAHA experiments yield individual $^3J_{HNH\alpha}$ and $^3J_{H\alpha CO}$ couplings for the $^1H^{\alpha 2}$ and $^1H^{\alpha 2}$ spins. These pairs of coupling constants, in combination with the value for $^3J_{HNCO}$, usually constrain the ϕ-angle. However, due to the symmetry about ϕ = 0 only its absolute value and not the sign can be determined without knowledge of the stereospecific assignment of the α-proton resonances. This is shown in Fig. 5 for residues Gly[82] and Gly[103] in flavodoxin. ϕ-angles around ±100 and ±60°, respectively, resulted from the measured vicinal couplings. On the basis of distance information provided by the different intensities of the two intraresidual $^1H^N$,$^1H^\alpha$ NOE peaks in a 3D ROESY-$^1H\{^{15}N\}$HMQC spectrum recorded with a mixing time of 33 ms (data not shown), the low-field $^1H^\alpha$ resonance of Gly[82] can be assigned to $H^{\alpha 3}$ (positive ϕ-angle) and the low-field $^1H^\alpha$ resonance of Gly[103] to $H^{\alpha 2}$ (negative ϕ-angle).

In conclusion, the coupled (H)NCAHA and (H)CANNH experiments presented here can be employed to measure all vicinal $^{1}H,^{1}H$ and $^{1}H,^{13}C$ couplings related to the backbone angle ϕ in proteins and serve to reduce ambiguities arising from the translation of coupling constants into structural information.

Acknowledgements

A grant from the Deutsche Forschungsgemeinschaft (Ru145/11-1) is gratefully acknowledged. The authors thank Prof. S. Mayhew, University College Dublin, and Martin Knauf for support in labeling and isolation of the *D. vulgaris* flavodoxin and Dr. J.M. Schmidt for helpful discussions.

References

Billeter, M., Neri, D., Otting, G., Qian, Y.Q. and Wüthrich, K. (1992) *J. Biomol. NMR*, **2**, 257–274.

Boucher, W., Laue, E.D., Campbell-Burk, S. and Domaille, P.J. (1992) *J. Am. Chem. Soc.*, **114**, 2262–2264.

Bystrov, V.F. (1976) *Prog. NMR Spectrosc.*, **10**, 41–81.

Bystrov, V.F., Gavrilov, Y.D. and Solkan, V.N. (1975) *J. Magn. Reson.*, **19**, 123–129.

Curley, G.P., Carr, M.C., Mayhew, S.G. and Voordouw, G. (1991) *Eur. J. Biochem.*, **202**, 1091–1100.

Delaglio, F., Torchia, D.A. and Bax, A. (1991) *J. Biomol. NMR*, **1**, 439–446.

Eggenberger, U., Karimi-Nejad, Y., Thüring, H., Rüterjans, H. and Griesinger, C. (1992a) *J. Biomol. NMR*, **2**, 583–590.

Eggenberger, U., Schmidt, P., Sattler, M., Glaser, S.J. and Griesinger, C. (1992b) *J. Magn. Reson.*, **100**, 604–610.

Emsley, L. and Bodenhausen, G. (1990) *Chem. Phys. Lett.*, **165**, 469–476.

Görlach, M., Wittekind, M., Farmer II., B.T., Kay, L.E. and Mueller, L. (1993) *J. Magn. Reson. Ser. B*, **101**, 194–197.

Griesinger, C., Sørensen, O.W. and Ernst, R.R. (1985) *J. Am. Chem. Soc.*, **107**, 6394–6396.

Griesinger, C., Sørensen, O.W. and Ernst, R.R. (1986) *J. Chem. Phys.*, **85**, 6837–6852.

Griesinger, C., Sørensen, O.W. and Ernst, R.R. (1987) *J. Magn. Reson.*, **75**, 474–492.

Grzesiek, S. and Bax, A. (1993) *J. Biomol. NMR*, **3**, 185–204.

Hansen, P.E. (1991) *Biochemistry*, **30**, 10457–10466.

Karplus, M. (1959) *J. Chem. Phys.*, **30**, 11–15.

Karplus, M. (1963) *J. Am. Chem. Soc.*, **85**, 2870–2871.

Kay, L.E., Brooks, B., Sparks, S.W., Torchia, D.A. and Bax, A. (1989) *J. Am. Chem. Soc.*, **111**, 5488–5490.

Kay, L.E., Ikura, M. and Bax, A. (1991) *J. Magn. Reson.*, **91**, 84–92.

Knauf, M.A., Löhr, F., Curley, G.P., O'Farrell, P., Mayhew, S.G., Müller, G. and Rüterjans, H. (1993) *Eur. J. Biochem.*, **213**, 167–184.

Logan, T.M., Olejniczak, E.T., Xu, R.X. and Fesik, S.W. (1993) *J. Biomol. NMR*, **3**, 225–231.

Ludvigsen, S., Andersen, K.V. and Poulsen, F.M. (1991) *J. Mol. Biol.*, **217**, 731–736.

Madsen, J.C., Sørensen, O.W., Sørensen, P. and Poulsen, F.M. (1993) *J. Biomol. NMR*, **3**, 239–244.

Marion, D., Ikura, M., Tschudin, R. and Bax, A. (1989) *J. Magn. Reson.*, **85**, 393–399.

Marion, D. and Wüthrich, K. (1983) *Biochem. Biophys. Res. Commun.*, **113**, 967–974.

Mayhew, S.G. and Tollin, G. (1992) In *Chemistry and Biochemistry of Flavoenzymes*, Vol. 3 (Ed, Müller, F.) CRC Press, Boca Raton, FL, pp. 389–426.

Montelione, G.T. and Wagner, G. (1990) *J. Magn. Reson.*, **87**, 183–188.

Montelione, G.T., Winkler, M.E., Rauenbuehler, P. and Wagner, G. (1989) *J. Magn. Reson.*, **82**, 198–204.

Morris, G.A. and Freeman, R. (1979) *J. Am. Chem. Soc.*, **101**, 760–762.

Schmieder, P. and Kessler, H. (1992) *Biopolymers*, **32**, 435–440.

Schmieder, P., Thanabal, V., McIntosh, L.P., Dahlquist, F.W. and Wagner, G. (1991) *J. Am. Chem. Soc.*, **113**, 6323–6324.

Schwalbe, H., Rexroth, A., Eggenberger, U., Geppert, T. and Griesinger, C. (1993) *J. Am. Chem. Soc.*, **115**, 7878–7879.

Seip, S., Balbach, J. and Kessler, H. (1992) *Angew. Chem.*, **104**, 1656–1658.

Shaka, A.J., Barker, P.B. and Freeman, R. (1985) *J. Magn. Reson.*, **64**, 547–552.

Shaka, A.J., Keeler, J., Frenkiel, T. and Freeman, R. (1983) *J. Magn. Reson.*, **52**, 335–338.

Sklenár, V. and Bax, A. (1987) *J. Magn. Reson.*, **74**, 469–479.

Sørensen, O.W. (1990) *J. Magn. Reson.*, **90**, 433–438.

Sørensen, O.W., Eich, G.W., Levitt, M.H., Bodenhausen, G. and Ernst, R.R. (1983) *Prog. NMR Spectrosc.*, **16**, 163–192.

Vuister, G.W. and Bax, A. (1992) *J. Biomol. NMR*, **2**, 401–405.

Vuister, G.W. and Bax, A. (1993) *J. Am. Chem. Soc.*, **115**, 7772–7777.

Wagner, G., Schmieder, P. and Thanabal, V. (1991) *J. Magn. Reson.*, **93**, 436–440.

Weisemann, R., Rüterjans, H., Schwalbe, H., Schleucher, J., Sattler, M., Bermel, W. and Griesinger, C. (1994a) *J. Biomol. NMR*, **4**, 231–240.

Weisemann, R., Löhr, F. and Rüterjans, H. (1994b) *J. Biomol. NMR*, **4**, 587–593.